JCI The Journal of Clinical Investigation

Disrupted Minor Intron Splicing Activates Reductive Carboxylation-mediated Lipogenesis to Drive Metabolic Dysfunction-associated Steatotic Liver Disease Progression

Yinkun Fu, … , Yimin Mao, Xu-Yun Zhao

J Clin Invest. 2025. https://doi.org/10.1172/JCI186478.

Research In-Press Preview Hepatology Metabolism

Graphical abstract

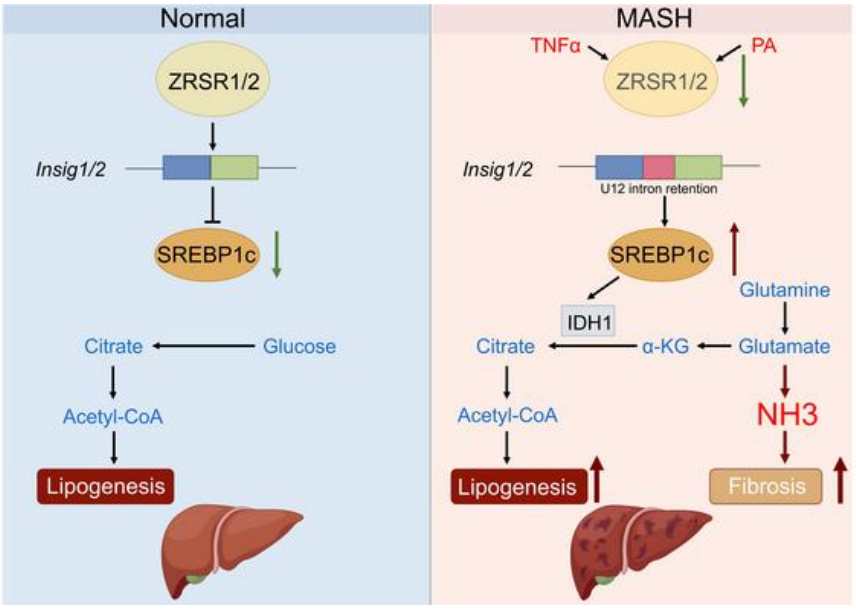

Disrupted Minor Intron Splicing Activates Reductive Carboxylation-mediated Lipogenesis to Drive Metabolic Dysfunction-associated Steatotic Liver Disease Progression

Yinkun Fu[1,2], Xin Peng[1], Hongyong Song[1], Xiaoyun Li[3], Yang Zhi[3], Jieting Tang[3], Yifan Liu[1], Ding Chen[1], Wenyan Li[1], Jing Zhang[2], Jing Ma[4], Ming He[2,5]*, Yimin Mao[3]* and Xu-Yun Zhao[1,4]*

[1] Department of Biochemistry and Molecular Cell Biology, Shanghai Key Laboratory for Tumor Microenvironment and Inflammation, Key Laboratory of Cell Differentiation and Apoptosis of National Ministry of Education, Shanghai Jiao Tong University School of Medicine, Shanghai, China.

[2] Institute for Translational Medicine on Cell Fate and Disease, Shanghai Ninth People's Hospital, Key Laboratory of Cell Differentiation and Apoptosis of National Ministry of Education, Department of Pathophysiology, Shanghai Jiao Tong University School of Medicine, Shanghai, China.

[3] Division of Gastroenterology and Hepatology, Renji Hospital, Shanghai Jiao Tong University School of Medicine; NHC Key Laboratory of Digestive Diseases; Shanghai Research Center of Fatty Liver Disease, Shanghai 200001, China.

[4] Department of Endocrinology and Metabolism, Renji Hospital, Shanghai Jiao Tong University School of Medicine, Shanghai, China.

[5] Department of Pathology, The Affiliated Hospital of Youjiang Medical University for Nationalities, Baise, China.

*To whom correspondence should be addressed:
Xu-Yun Zhao, Ph.D. 280 Chongqing South Rd, Shanghai Jiao Tong University School of Medicine, Shanghai, China. Email: xuyunzhao@shsmu.edu.cn.
Yimin Mao, M.D. 145 Zhongshan Mid Rd, Renji Hospital, Shanghai Jiao Tong University School of Medicine, Shanghai, China. Email: maoym11968@163.com.
Ming He, Ph.D. 280 Chongqing South Rd, Shanghai Jiao Tong University School of Medicine, Shanghai, China. Email: heming@shsmu.edu.cn.

Competing interests: The authors declare that they have no competing interests.

Abstract

Aberrant RNA splicing is tightly linked to diseases, including metabolic dysfunction-associated steatotic liver disease (MASLD). Here, we revealed that minor intron splicing, a unique and conserved RNA processing event, is largely disrupted upon the progression of metabolic dysfunction-associated steatohepatitis (MASH) in mice and humans. We demonstrated deficiency of minor intron splicing in the liver induces MASH transition upon obesity-induced insulin resistance and LXR activation. Mechanistically, inactivation of minor intron splicing leads to minor intron retention of *Insig1* and *Insig2*, resulting in premature termination of translation, which drives proteolytic activation of SREBP1c. This mechanism is conserved in human patients with MASH. Notably, disrupted minor intron splicing activates glutamine reductive metabolism for *de novo* lipogenesis through the induction of Idh1, which causes the accumulation of ammonia in the liver, thereby initiating hepatic fibrosis upon LXR activation. Ammonia clearance or IDH1 inhibition blocks hepatic fibrogenesis and mitigates MASH progression. More importantly, the overexpression of *Zrsr1* restored minor intron retention and ameliorated the development of MASH, indicating that dysfunctional minor intron splicing is an emerging pathogenic mechanism that drives MASH progression. Additionally, reductive carboxylation flux triggered by minor intron retention in hepatocytes serves as a crucial checkpoint and potential target for MASH therapy.

Introduction

Metabolic dysfunction-associated steatotic liver disease (MASLD), previously termed nonalcoholic fatty liver disease (NAFLD), is a clinicopathological condition that is increasingly recognized as a component of the epidemic of obesity. It causes a spectrum of liver damage, ranging from simple fatty liver with uncomplicated steatosis to progressive metabolic dysfunction-associated steatohepatitis (MASH), which increases the risk of fibrosis and cirrhosis. It is estimated that more than 25% of the adult population worldwide has fatty liver, and approximately 5-10% of these individuals further progress to MASH (1-3). MASLD is rapidly emerging as a leading etiology for chronic liver disease and a common indication for adult liver transplantation. Notably, the prevalence of MASLD is expected to increase worldwide along with the increasing incidence of obesity and type 2 diabetes mellitus (T2DM) due to the lack of effective pharmacotherapies (4, 5). An increase in hepatic steatosis is a hallmark of MASLD progression. More importantly, the pathogenic consequences of the MASH transition, such as hepatic fibrosis, cirrhosis and hepatocyte death, are largely implicated in the mortality and the prognosis of MASH and are ultimately irreversible (6-9). Therefore, blocking the MASH transition is a critical intervention for the pathogenesis of MASH.

RNA splicing is a fundamental biological process that is mediated by a special group of RNA-binding proteins that control the posttranscriptional processing of RNA and generate protein diversity (10, 11). However, abnormal RNA splicing

has become a pathological factor in diverse diseases (12, 13). The splicing of introns depends on the terminal dinucleotides of the intron, which include GT-AG/GC-AG and AT-AC and refer to major (U2-type) and minor (U12-type) introns, respectively. While major introns are universally present in the majority of genes, minor introns are rare and exist in only a minor class of genes (<0.4% of all introns), however, they are highly conserved and function in various indispensable biological pathways (14). Recent studies revealed that dysregulation of the RNA splicing machinery is important for the development of MASLD (12, 15-17). The minor intron splicing factors zinc finger CCCH-type, RNA binding motif and serine/arginine rich 1/2 (*Zrsr1* and *Zrsr2*) are highly conserved paralogs that recognize a unique splice site of minor introns upon splicing (18). In humans, *ZRSR2* is the dominant minor intron splicing factor since *ZRSR1* is considered a pseudogene, whereas in mice, both *Zrsr1* and *Zrsr2* are required for minor intron splicing (19). Mutations in *Zrsr1* or *Zrsr2* cause retention of most of the minor introns, which is associated with multiple diseases, including developmental disorders (19-22), neurodegeneration (23), and cancer (24). Although the pivotal role of major intron splicing in driving MASLD progression has been elucidated, how minor intron splicing is implicated in MASH pathogenesis needs further investigation.

De novo lipogenesis is a metabolic process that is closely associated with hepatic steatosis and MASH pathogenesis. In a conventional view, hepatocytes use acetyl-CoA generated by the glycolysis pathway for the *de novo* synthesis of

fatty acids and lipids, whereas under certain conditions, such as hypoxia, glutamine is reductively carboxylated to citrate to produce lipogenic carbon (25). Notably, during cancer development, glutamine is frequently absorbed and reductively carboxylated to synthesize lipids to fulfill the demand for energy storage and cell proliferation (26). Targeting glutaminolysis has been proven to inhibit tumorigenesis by suppressing lipid synthesis (27). The relationship between MASH progression and aberrant stimulation of hepatic *de novo* lipogenesis has been firmly established in previous studies (28, 29). Sterol regulatory element-binding protein 1c (*Srebp1c*) is a central regulator of the hepatic lipogenic gene program, which includes fatty acid synthase (*Fasn*) and stearoyl-CoA desaturase 1 (*Scd1*) (30, 31). Liver X receptor (*Lxr*), a nuclear hormone receptor, directly binds to the *Srebp1c* promoter and modulates *Srebp1c* expression. It is documented that LXR-mediated SREBP1c activity is highly stimulated during MASH progression (32). Treatment with the LXR agonist T0901317 results in severe hypertriacylglycerolemia and hepatic triacylglycerol accumulation, whereas treatment with the LXR antagonist SR9238 blocks MASH progression (33). During the development of MASLD, an increased amount of SREBP1c proteins is processed to their active forms in the Golgi apparatus by protease cleavage. Insulin induced gene 1 and 2 (*Insig1* and *Insig2*) are ER-localized polytopic membrane proteins that bind SREBP cleavage-activating protein (SCAP) and prevent it from escorting SREBP1c to the Golgi apparatus for proteolytic processing (34-37). Loss of INSIG proteins is largely implicated in MASH and cancer progression (38, 39).

In this study, we revealed that minor intron splicing is profoundly inactivated during MASH development. The depletion of *Zrsr1* and *Zrsr2*, two essential minor intron splicing factors in the liver, directly induces hepatic steatosis and further promotes MASH progression upon obesity-induced insulin resistance and LXR activation. Deficiency of *Zrsr1* and *Zrsr2* in the liver triggers *Insig1* and *Insig2* minor intron retention for premature termination of translation, thereby constantly activating SREBP1c. Metabolomics and isotope-labeled metabolite flux analyses support the notion that the dominant carbon source in the liver for lipogenesis switches to glutamine, and surprisingly, it undergoes SREBP1c-induced isocitrate dehydrogenase 1 (IDH1)-mediated reductive carboxylation upon inactivation of minor intron splicing. This metabolic remodeling is critical in MASH progression due to the overflow of ammonia production in the liver. Clearance of ammonia or suppression of IDH1 activity reverses hepatic fibrosis and MASH progression. Herein, we demonstrated an unexpected role of minor intron splicing inactivation in MASH progression through the induction of SREBP1c nuclear form processing. Minor intron splicing deficiency augments glutamine-derived lipogenic carbon by inducing reductive carboxylation flux for *de novo* lipogenesis. Thus, this LXR-SREBP1c-IDH1-mediated reductive carboxylation pathway may serve as a pivotal and unique checkpoint for MASH progression and a promising target for MASH therapy.

Results

Minor intron retention caused by reduction of *Zrsr1* and *Zrsr2* in the liver promotes MASH progression.

The deficiency of RNA splicing is tightly linked to MASLD progression. However, whether minor intron splicing is disrupted in the MASH liver is unclear. Here, we performed RNA sequencing analyses of livers from chow- and CDA-HFD (choline-deficient, L-amino acid-defined high-fat diet, also called MASH diet)-fed mice and compared the occurrence rates of minor (U12) and major (U2) intron retention in the liver according to the minor intron database (40). The results revealed that the fold change of the amounts of both minor (U12) intron and major (U2) intron reads significantly increased in the livers of the mice after MASH diet feeding (Figure 1A). Interestingly, among the 657 minor introns found within 606 recognized genes that contain minor introns, a substantial 46% of these minor introns were retained. In contrast, out of the 211,005 major introns present in 32,396 known genes with major introns, only 3.5% of these major introns were retained, suggesting that minor intron retention is a common RNA splicing deficiency event in the MASH liver (Figure 1B). The dysregulation of minor intron splicing factors leads to minor intron retention. Among all the minor intron splicing factors and snRNAs, the expression of *Zrsr1* and *Zrsr2*, which recognize the consensus splice site of the minor intron, is extensively reduced in the livers of mice after MASH diet feeding (Figure 1C-D and S1A). In addition, an RNA sequencing dataset (GSE126848) of healthy and MASH human liver samples as well as qPCR analyses of collected liver biopsies from MASH patients further confirmed that the expression of *ZRSR2*, the major minor intron

splicing factor in humans, is suppressed in patients with MASH (Figure 1E, Figure S1B and Table S1). Excess fatty acid accumulation and severe inflammation in the liver facilitate MASH progression. Notably, treating primary hepatocytes with palmitic acid (PA) in combination with the inflammatory cytokine tumor necrosis factor-α (TNFα) significantly downregulated *Zrsr1* expression and slightly decreased *Zrsr2* expression (Figure 1F-G). These results indicate that the downregulation of *Zrsr1* and *Zrsr2* in the MASH liver may cause minor intron retention.

To investigate the consequences of the reduction in *Zrsr1* and *Zrsr2*, we took advantage of CRISPR/CAS9 editing strategy to generate a *Zrsr1* and *Zrsr2* double-deficient mouse model (ZLKO) via the injection of adeno-associated virus (AAV), which carried two small guide RNA (sgRNA) pairs targeting *Zrsr1* and *Zrsr2*, as indicated, into a *Cas9* transgenic mouse line (Figure 1H). The ZLKO mouse model offers a distinct advantage by effectively circumventing the potential compensatory effects that might occur when either *Zrsr1* or *Zrsr2* is depleted individually, as previously reported (41). After AAV-sgRNA virus injection, *Zrsr1* and *Zrsr2* were both largely depleted in the liver but not in other tissues. Additionally, the inactivation of *Zrsr1* and *Zrsr2* was highly restricted to hepatocytes (Figure S1C-H). To verify whether minor intron splicing was compromised by *Zrsr1* and *Zrsr2* depletion, we analyzed RNA sequencing data from the livers of ZLKO and control mice. The fold change in the amounts of minor (U12) intron reads significantly increased, whereas that of major (U2)

intron reads slightly increased in the livers of ZLKO mice (Figure 1I). Among the 657 minor introns in 606 minor intron-containing genes, 56% were retained, whereas only 0.3% of the 211,005 major introns in 32,396 known major intron-containing genes showed retention, indicating that *Zrsr1* and *Zrsr2* abrogation mainly leads to minor intron retention (Figure 1J and Table S2). We subsequently analyzed the metabolic phenotype of the ZLKO mice. Compared with those of control mice, the livers of ZLKO mice were heavier and contained more lipid droplets, as shown by H&E and Oil Red O staining, while the body weights of these mice were equal (Figure 1K and Figure S2A). Then, we measured liver and plasma triglyceride and cholesterol contents in control and ZLKO mice. The liver triglyceride and cholesterol levels of the ZLKO mice were significantly elevated, but the plasma triglyceride and cholesterol levels in these mice remained unaltered (Figure 1L-M and Figure S2B). Elevated hepatic triglyceride accumulation may be driven by insulin resistance. Therefore, we measured the glucose content and insulin sensitivity of the control and ZLKO mice. Although the *ad lib* glucose level was unchanged in the ZLKO mice, the mice exhibited slightly enhanced insulin sensitivity, as indicated by the glucose tolerance test (GTT), and the insulin level was slightly lower in the ZLKO mice (Figure S2C-E). These results indicate that the loss of *Zrsr1* and *Zrsr2* directly leads to a hepatic steatosis phenotype independent of insulin resistance.

The onset of hepatic steatosis is a crucial risk factor in the advancement of MASLD. Notably, Sirius red staining and alanine aminotransferase (ALT) and

aspartate aminotransferase (AST) measurements indicated that hepatic fibrogenesis and injury were initiated in the livers of ZLKO mice (Figure 1K and N). Insulin resistance is a well-known driver of MASLD progression. High-fat diet (HFD)-induced obesity impairs glucose homeostasis and leads to insulin resistance. To further explore the role of minor intron splicing in obesity-induced insulin resistance, ZLKO and control mice were fed on HFD for 10 weeks (Figure 1O). The ZLKO mice gained less weight than the control mice (Figure 1P) but had heavier livers (Figure S3A), and the liver triglyceride content was largely elevated, while the plasma triglyceride, cholesterol, non-esterified fatty acid (NEFA) and β-hydroxybutyrate contents were not affected (Figure 1Q-R and Figure S3B-D). The food intake of the ZLKO mice during HFD feeding was not affected (Figure S3E). Additionally, the plasma glucose and insulin levels were not altered in the ZLKO mice (Figure S3F-G). Moreover, the results of the GTT and insulin tolerance test (ITT) also revealed no differences between the control and ZLKO mice after HFD feeding (Figure S3H), suggesting that the control and ZLKO mice have similar degrees of insulin resistance during diet-induced obesity. Liver histology and Oil Red O staining revealed more severe hepatic steatosis in the livers of ZLKO mice after HFD feeding than in those of control mice (Figure 1S). Although brown adipose tissue (BAT) histology and thermogenesis-related gene expression did not differ, epididymal white adipose tissue (eWAT) presented more multilocular structures and increased expression of thermogenic genes, indicating that more beige fat formed in ZLKO mice upon HFD feeding (Figure 1S and Figure S3I-J). This phenotype is strongly associated

with restricted body weight gain in HFD-fed ZLKO mice. In contrast, the ZLKO mice fed on low-fat diet had no difference in body weight gain (Figure S3K) while the thermogenic gene expression was unchanged in both BAT and eWAT, suggesting that beige fat formation in the eWAT of ZLKO mice is a unique event during obesity development (Figure S3L-M). Intriguingly, although the ZLKO mice is leaner after HFD feeding, the MASH phenotype, including liver collagen deposition and the degree of injury, was significantly augmented, as revealed by Sirius red staining and ALT and AST levels (Figure 1S-T). These results imply that minor intron retention leads to accelerated MASH progression in obesity-induced insulin resistance conditions.

Minor intron retention activates SREBP1c-mediated *de novo* lipogenesis, which results in the progression of MASH upon LXR activation.

To explore the potential pathways regulated by minor intron splicing deficiency, we analyzed RNA sequencing data from the livers of control and ZLKO mice. Overall, depletion of *Zrsr1* and *Zrsr2* led to more genes being upregulated than downregulated (Figure S4A). Then, we clustered genes upregulated or downregulated >1.4-fold via DAVID clustering analysis (https://david.ncifcrf.gov/). The results showed a drastic enrichment of upregulated genes in the SREBP signaling pathway, which mainly regulates hepatic *de novo* lipogenesis, while the downregulated genes were clustered into lipid catabolism-associated pathways (Figure 2A and Figure S4B). Moreover, the expression of a gene set that regulates the *de novo* lipogenesis pathway was also highly increased (Figure

2B). QPCR analyses revealed that the expression of the lipogenic genes *Srebp1c* and *Scd1* was increased in the livers of ZLKO mice while the expression of genes regulating lipid formation did not change (Figure 2C). Interestingly, the expression of genes involved in fatty acid oxidation and inflammation was slightly downregulated, whereas the expression of genes linked to fibrosis was stimulated, suggesting that the induction of fibrosis in the livers of ZLKO mice may be uncoupled from the inflammatory state (Figure 2D-E). Immunoblotting revealed that *Srebp1c* expression and cleavage were augmented after depleting *Zrsr1* and *Zrsr2*. The phosphorylation and total level of adenosine 5'-monophosphate-activated protein kinase (AMPK), which regulates *de novo* lipogenesis, were not affected (Figure 2F and Figure S4C). Consistently, after HFD feeding, the expression of the upregulated lipogenic genes *Scd1*, *Fasn*, lipid formation genes, fat-specific protein 27 (*Fsp27*) and peroxisome proliferator-activated receptor γ (*Pparγ*) further increased together with the increase of inflammatory and fibrogenesis-related genes in ZLKO mice (Figure 2G-H). Western blot analysis revealed that precursor and cleaved SREBP1c levels were increased in obese ZLKO mice. Since obesity increases immune cell infiltration in the liver, which elevates c-Jun N-terminal kinase (JNK) signaling, we further measured the phosphorylation of JNK. Western blot analysis revealed that the expression of phosphorylated JNK was increased, further suggesting that minor intron splicing deficiency triggers hepatic inflammation and further exacerbates fibrosis during obesity development. The levels of phosphorylated and total

AMPK were equal, which was consistent with the results of the chow-fed group (Figure 2I and Figure S4D).

The nuclear receptor LXRα/β binds retinoid X receptor (RXR) α/β to form a heterodimer that transcriptionally induces *Srebp1c* expression. To investigate whether minor intron splicing directly modulates SREBP1c activity, we gavaged control and ZLKO mice with SR9238, an LXR antagonist, to suppress LXR activity (Figure S5A). The SR9238 treatment in wild type mice significantly decreased the expression of hepatic lipogenic genes (Figure S5B). Conversely, in ZLKO mice, despite treatment with SR9238, the levels of liver triglycerides and cholesterol remained significantly higher compared to those of control-treated mice (Figure S5C-F). In addition, although the upregulation of *Srebp1c* mRNA in the livers of ZLKO mice was largely suppressed, the expression of cleaved SREBP1c was still increased in ZLKO mice, which suggests that minor intron splicing may directly control SREBP1c nuclear form processing. This notion is further supported by the induction of the SREBP1c target gene *Scd1* and the lipid marker *Fsp27* (Figure S5G-H). The aberrant activation of LXR/RXR complex activity during obesity is emerging as a vital cause of MASLD and facilitates MASH progression. To investigate whether minor intron splicing plays an important role in LXR-SREBP1c-mediated MASLD progression, we gavaged the LXR agonist T0901317 (T1317) in control and ZLKO mice (Figure 2J). In wild type mice, T1317 treatment highly induced the expression of hepatic lipogenic genes (Figure S5I). Of note, T1317-treated ZLKO mice exhibited more severe

liver steatosis as well as elevated liver weights and plasma and hepatic triglyceride and cholesterol levels (Figure 2K and Figure S5J-K). Notably, the livers of the ZLKO mice became fibrotic after T1317 treatment, as shown by liver morphology and Sirius red staining (Figure 2L). Gene expression analyses revealed that inflammatory genes such as C-C motif chemokine ligand 2 (*Ccl2*), *Ccl5* and interleukin-1β (*Il1β*) and fibrotic genes such as collagen 1a1 (*Col1a1*), *Col1a2* and *Col3a1* were dramatically upregulated. The expression of the lipogenic genes *Srebp1c*, *Fasn* and *Scd1* was not further induced, probably due to the increase in inflammation in the liver, which suppressed the lipogenic program. However, the lipid marker *Fsp27* was increased, which was associated with enhanced lipid deposition in the livers of ZLKO mice (Figure 2L-N). Western blot analyses indicated that the expression of premature SREBP1c was equal but that the active form of SREBP1c was more abundant in ZLKO mice after T1317 treatment. The phosphorylation of the immune-associated nuclear factor kappa-B (NF-κB) P65 subunit and the activation of JNK were highly induced, suggesting that inflammation is extensively triggered in the liver. Additionally, the increase in cleaved caspase 3 indicated that apoptosis was induced in the ZLKO mouse liver after T1317 treatment (Figure 2O). The increase in inflammation and fibrosis in the *Zrsr1* and *Zrsr2* double-deficient livers led to liver damage and the MASH phenotype, which was supported by the increase in ALT and AST levels and hydroxyproline deposits in the livers of these mice (Figure 2P-Q). These results indicate that inactivation of minor intron splicing directly triggers SREBP1c processing, which promotes hepatic lipid accumulation. More importantly, the

MASH phenotype is induced in the liver with minor intron retention upon LXR activation.

The minor intron retention of the *Insig1* and *Insig2* genes promotes SREBP1c proteolytic activation.

To explore the mechanism by which disrupted minor intron splicing activates SREBP1c processing, we further analyzed the expression and function of minor intron-retained genes via RNA sequencing. The expression of these genes was mostly upregulated, and their function was strongly related to protein localization of the endoplasmic reticulum (ER) and intracellular protein trafficking (Figure 3A-B). Among them, Insig1 and Insig2 are classic inhibitors of *de novo* lipogenesis that function by anchoring the premature SREBP1c protein in the ER. We speculate that the minor intron retention of *Insig1* and *Insig2* may affect SREBP1c proteolytic activation. Through the UCSC Genome Browser, we revealed that there were increased peaks in the minor intron region of the *Insig1* and *Insig2* genes in ZLKO mice but not in adjacent major introns. The StringTie program reconstitutes a new transcript of *Insig1* and *Insig2*, which is generated due to the retention of minor introns (Figure 3C-D and Figure S6A). Furthermore, we verified that the expression of minor introns in *Insig1* and *Insig2* was substantially increased in ZLKO mice, while the expression of wild type *Insig1* was decreased (Figure 3E-H). The minor introns retained in the *Insig1* and *Insig2* transcripts contain alternative stop codons for premature termination of translation (Figure S6A). Western blot analysis revealed that the expression of

Insig1 decreased upon *Zrsr1* and *Zrsr2* depletion (Figure 3I). To investigate whether deficiency of minor intron splicing cell-autonomously mediates hepatic *de novo* lipogenesis through *Insig1* and *Insig2* minor intron retention, we substantially depleted *Zrsr1* and *Zrsr2* in an AML12 mouse normal hepatic cell line and primary hepatocytes via the CRISPR/CAS9 editing strategy. *Zrsr1* and *Zrsr2* sgRNA- and *Cas9*-transduced AML12 cells and primary hepatocytes (KO) presented increased *Insig1* and *Insig2* minor intron signals and decreased wild type *Insig1* mRNA and protein expression (Figure 3J-L and Figure S6B), while the expression of the *de novo* lipogenic genes *Srebp1c*, *Fasn* and *Scd1* was induced, as was SREBP1c cleavage. This effect was further amplified by LXR activation (Figure 3M-N and Figure S6C). In addition, no significant change in the activation of AMPK was observed (Figure 3N). Notably, adenoviral overexpression of *Insig1* reversed *Zrsr1*- and *Zrsr2*-double deficiency-induced SREBP1c activation under both basal and LXR antagonist-treated conditions, indicating that the minor intron retention of *Insig* genes is the main factor that causes SREBP1c processing in ZLKO mice (Figure 3O-P). We next explored whether decreased *Zrsr1* and *Zrsr2* expression in the MASH stage further drives the minor intron retention of *Insig1* and *Insig2*. We measured the expression of minor introns of *Insig1* and *Insig2* in the livers of mice fed a MASH diet and in human MASH patients. The results showed that the minor intron expression of *Insig1* and *Insig2* was largely elevated in mice and humans at the MASH stage while the expression of wild type Insig1 was reduced (Figure 3Q-R). Western blot analysis confirmed that INSIG1 protein expression was decreased and that

SREBP1c processing was increased in the livers of mice at the MASH stage (Figure 3S). Notably, primary hepatocytes treated with PA and TNFα alone presented increased minor intron expression of *Insig1* and *Insig2*, which was more significantly induced upon PA and TNFα treatment in combination, while the expression of wild type Insig1 mRNA and protein was suppressed by PA and TNFα treatment alone or in combination. Consequently, SREBP1c cleavage is increased (Figure 3T-V). Taken together, these results provide evidence that hepatic minor intron retention of the *Insig1* and *Insig2* genes upon *Zrsr1* and *Zrsr2* depletion and at the MASH stage leads to SREBP1c proteolytic activation.

Dysfunction of minor intron splicing induces glutamine reductive carboxylation flux for *de novo* lipogenesis by activating IDH1.

Increased hepatic *de novo* lipogenesis may disrupt metabolic homeostasis in mice with minor intron splicing deficiency to promote MASH progression. Thus, we performed a metabolomics analysis of the livers of control and ZLKO mice after T1317 treatment to evaluate whether metabolic remodeling upon minor intron splicing inactivation triggered MASH progression. *De novo* lipogenesis generally incorporates acetyl-CoA generated by glycolysis into fatty acids, however, our metabolomics results imply that the increased metabolites in *Zrsr1* and *Zrsr2* double-deficient livers are enriched in amino acid metabolism and the urea cycle (Figure 4A). The glycolysis and pentose phosphate pathways, which regularly contribute to *de novo lipogenesis*, were not significantly altered (Figure 4B). Intriguingly, the tricarboxylic acid cycle (TCA) cycle intermediates citrate and

α-ketoglutarate (α-KG), and the adenosine triphosphate (ATP)/ADP and nicotinamide adenine dinucleotide (NADH)/NAD ratios increase, indicating that a lipogenic environment is formed in the livers of ZLKO mice (Figure 4C-D). Based on [U-^{14}C]-labeled acetate tracing experiments, we further confirmed that the disruption of minor intron splicing in hepatocytes increased the *de novo* synthesis of fatty acids from acetate-derived acetyl-CoA, however, [U-^{14}C]-labeled glucose utilization for *de novo* lipogenesis decreased, especially upon LXR activation, suggesting that glycolysis is not the major carbon source for *de novo* lipogenesis induced by minor intron splicing deficiency (Figure 4E-F). The increase in urea cycle metabolites suggested elevated amino acid degradation, which may serve as an alternative carbon source for *de novo* lipogenesis (Figure 4G). To verify this hypothesis, we used [U-^{13}C]-labeled glutamine, one of the most abundant amino acids, as a tracer to assess the incorporation of amino acid-derived acetyl-CoA into *de novo* synthesized fatty acids. The calculated lipogenic acetyl-CoA contribution was increased in Zrsr1 and Zrsr2 double-inactivated hepatocytes, suggesting that amino acid metabolism-mediated lipogenesis was induced (Figure 4H). Interestingly, total ^{13}C-labeled monounsaturated fatty acids (C16:1 and C18:1) but not saturated fatty acids (C16:0 and C18:0) were significantly increased in *Zrsr1* and *Zrsr2* double-deficient hepatocytes under both basal and LXR activated conditions (Figure 4I). However, mass isotopomer distribution analysis revealed that M+4, M+6 and M+8-labeled palmitate (C16:0), which represent palmitate containing 2, 3 and 4 acetyl-CoA molecules derived from [U-^{13}C] glutamine, respectively, were increased by minor intron splicing disruption,

while M+2 to M+6-labeled palmitoleic acid (C16:1) was more profoundly increased along with a decrease in unlabeled (M+0) palmitoleic acid in *Zrsr1* and *Zrsr2* double-deficient hepatocytes, implying a high preference for glutamine-derived lipogenic carbon usage for monounsaturated fatty acid synthesis through *de novo* lipogenesis upon minor intron splicing deficiency. The activation of LXR specifically increased the formation of monounsaturated fatty acids from glutamine (Figure 4J). Amino acids can be metabolized into TCA cycle intermediates to oxidatively generate citrate, which is used for *de novo* lipogenesis. Under certain conditions, amino acids, especially glutamine, undergo reductive carboxylation to generate citrate (Figure 4K). To determine the metabolic route through which glutamine generates citrate for *de novo* lipogenesis in minor intron splicing-deficient hepatocytes, we performed a metabolic flux assay using a [U-^{13}C]-labeled glutamine tracer to analyze the amount of oxidatively and reductively synthesized citrate. The enrichment of M+4-labeled citrate, fumarate and malate, which represent the oxidative pathway of glutamine metabolism, was attenuated. LXR activation further inhibited this oxidative route of citrate synthesis from glutamine (Figure 4L). Then, we measured M+5-labeled citrate, which represents the citrate derived from glutamine through reductive carboxylation. The M+5-labeled citrate and the M+5/M+4-labeled citrate ratio increased in minor intron splicing inactivated hepatocytes. In addition, T1317 treatment further elevated the reductive carboxylation of glutamine (Figure 4M).

IDH1 and IDH2 are key dehydrogenases located in the cytosol and mitochondria, respectively, that catalyze the reductive metabolism of α-KG to citrate. A previous report revealed that SREBP signaling regulates *Idh1* expression (42). Here, we also observed that *Idh1* expression was increased in the livers of ZLKO mice at both the mRNA and protein levels, while *Idh2* expression was not altered (Figure 4N-O and Figure S7A). The induction of *Idh1* but not *Idh2* was also confirmed in AML12 cells with minor intron splicing defects. The expression of *Idh1* was further augmented under LXR-activated conditions (Figure 4P-Q). Furthermore, the overexpression of *Srebp1c* in AML12 cells directly increased the expression of *Idh1* and the lipogenic gene *Scd1*, which was further elevated by T1317 treatment (Figure 4R). The upregulation of *Idh1* expression was also observed in the livers of MASH patients (Figure 4S). Interestingly, *Insig1* overexpression by adenoviral transduction rescued the increase in *Idh1* expression in minor intron splicing-deficient primary hepatocytes, further confirming that dysfunctional minor intron splicing induces *Idh1* expression through SREBP1c activation (Figure 4T). Notably, suppressing IDH1 activity via the IDH1 inhibitor GSK864 attenuated basal and stimulated M+5-labeled citrate production and the M+5/M+4-labeled citrate ratio in hepatocytes deficient in minor intron splicing upon T1317 treatment (Figure 4U). As a result, *de novo* lipogenesis, as indicated by [U-^{14}C]-labeled acetate flux, was obviously blocked (Figure 4V). Taken together, these results support that the stimulation of SREBP1c activity in minor intron-splicing-inactivated hepatocytes drives the reductive carboxylation of glutamine to generate lipogenic carbon for *de novo* lipogenesis through the induction of *Idh1*

expression.

IDH1-mediated glutamine reductive carboxylation flux induces hepatic fibrogenesis via ammonia-driven activation of hepatic stellate cells.

MASH progression is accompanied by increased fibrosis. However, how enhanced *de novo* lipogenesis triggers hepatic fibrogenesis is still controversial. The reductive carboxylation-mediated lipogenesis that occurs upon minor intron splicing deficiency may reshape the local liver microenvironment to induce hepatic stellate cell activation. Glutamine contains two amino groups that efficiently transport ammonia in circulation to the liver for clearance by the urea cycle. The conversion of glutamine to α-KG for reductive carboxylation may release a significant amount of ammonia and increase the urea cycle flux. It is possible that overwhelming ammonia accumulation in the liver results in over the capacity of liver detoxification in ZLKO mice, thus leading to MASH progression. Here, we found that the ammonia concentration is increased in minor intron splicing-deficient hepatocytes and further augmented upon LXR activation (Figure 5A). Furthermore, mice with a loss of minor intron splicing activity presented a significantly elevated ammonia content in the liver under normal, obese and LXR-activated conditions (Figure 5B). Notably, the hepatic ammonia content drastically increased in the mice in the MASH stage (Figure 5C). The staining of ammonia by Nessler's reagent supported the increase in ammonia deposition in the livers of ZLKO mice upon LXR activation, and more importantly, the ammonia-stained area was strongly associated with collagen deposition, as

indicated by Sirius red staining of the liver (Figure 5D). Hepatic stellate cells (HSCs) largely contribute to collagen production in the liver. Therefore, we performed a co-culture experiment using transwells, which allows ammonia secreted from minor intron splicing-defective hepatocytes to influence co-cultured HSCs (Figure 5E). The results revealed that the secreted product of *Zrsr1* and *Zrsr2* double-inactivated hepatocytes induced HSC collagen gene expression upon T1317 treatment (Figure 5F). Furthermore, ammonium chloride treatment dose-dependently induced collagen gene expression in HSCs (Figure 5G). L-ornithine-l-aspartate (LOLA) is a reagent capable of lowering hepatic ammonia by enhancing the urea cycle (43). We then pretreated ZLKO mice with LOLA or the control for 17 days and subsequently in combine with the activation of LXR via T1317 treatment (Figure 5H). LOLA treatment specifically attenuated the hepatic ammonia content without affecting body weight, liver weight, liver or plasma triglyceride levels or cholesterol content in the ZLKO mice (Figure 5I and Figure S7B-E). As a consequence, hepatic fibrosis was reduced, whereas liver steatosis, inflammation and injury were not affected (Figure 5J and Figure S7F). The expression of collagen genes decreased upon LOLA treatment in ZLKO mice, suggesting a decrease in hepatic HSC activation, while lipogenesis- and inflammation-associated gene expression was not influenced (Figure 5K and Figure S7G-H). Idh1 has been shown to be the critical enzyme that regulates reductive carboxylation flux and ammonia production in the livers of minor intron splicing-deficient mice. Thus, we further investigated whether the inhibition of IDH1 is sufficient to block minor intron splicing deficiency-induced MASH

progression. We intraperitoneally injected the IDH1 inhibitor GSK864 or the control into ZLKO mice and treated them with T1317 (Figure 5L). The body weight and liver weight of the GSK864-treated ZLKO mice obviously decreased, and the liver triglyceride and plasma triglyceride contents and cholesterol content also drastically reduced (Figure 5M and Figure S7I-K), suggesting that reductive carboxylation-mediated *de novo* lipogenesis in the liver was suppressed. More importantly, hepatic ammonia levels in ZLKO mice were reduced after GSK864 treatment, probably due to the reversal of glutamate deamination (Figure 5N). As a result, hepatic steatosis, fibrosis and ammonia accumulation were largely diminished in the livers of the IDH1 activity-inhibited ZLKO mice (Figure 5O). Therefore, liver injury, as indicated by the ALT and AST levels, was attenuated (Figure 5P). Notably, the expression of hepatic inflammation- and fibrosis-associated genes was profoundly suppressed, supporting the amelioration of minor intron splicing deficiency-induced MASH progression after treatment with GSK864 (Figure 5Q-R). The expression of lipogenic markers and SREBP1c processing were not altered, however, the lipid marker *Fsp27* was significantly reduced (Figure 5S and Figure S7L). These results led to the conclusion that the increase in IDH1 activity upon minor intron splicing deficiency enhances hepatic ammonia production by inducing the reductive carboxylation flux of glutamine, which initiates HSC activation and hepatic fibrogenesis. Inhibition of IDH1 activity efficiently reduces the minor intron splicing inactivation-induced MASH phenotype upon LXR activation.

The restoration of minor intron splicing activity, or the targeting of the IDH1-ammonia axis in the liver ameliorates MASH progression.

Our previous results demonstrated that the downregulation of Zrsr1 and Zrsr2 in the liver leads to minor intron retention, which triggers the activation of the SREBP1c-IDH1-ammonia axis to induce MASH progression. To explore whether intervention with minor intron splicing factors or the IDH1-ammonia axis blocks MASH progression, we overexpressed Zrsr1 in the hepatocytes of mice via AAV under the liver-specific thyroxine-binding globulin (TBG) promoter and subjected the mice to MASH diet feeding to explore whether reactivating minor intron splicing mitigates MASH progression (Figure 6A). Hepatic overexpression of Zrsr1 reversed the minor intron retention of Insig1 and Insig2 in the livers of mice with MASH (Figure S8A-B). Although Zrsr1 overexpression in the livers of the mice did not affect body weight, the glucose level was slightly reduced (Figure S8C-D). Notably, liver weight gain and hepatic triglyceride accumulation were reversed in hepatic Zrsr1-overexpressing mice, but the hepatic cholesterol level remained unchanged, while the plasma triglyceride and cholesterol levels were unaltered (Figure 6B-C and Figure S8E-F). After MASH diet feeding, the livers of the Zrsr1-overexpressing mice appeared to be smaller and smoother in morphology. Liver histology, Oil Red O and Sirius red staining suggested that the overexpression of *Zrsr1* in the liver impeded MASH progression, as indicated by the blockade of steatosis, inflammation, fibrosis and ammonia accumulation (Figure 6D-E). The cleavage of the SREBP1c precursor, reduction in *Insig1* expression and increase in *Idh1* expression due to minor intron splicing

inactivation in MASH were significantly reversed by *Zrsr1* overexpression (Figure 6F and Figure S8G). Consistently, the expression of genes associated with lipogenesis, inflammation and fibrosis was obviously suppressed, indicating that the MASH phenotypes were extensively relieved (Figure 6G). Additionally, liver damage, as indicated by ALT and AST levels, was reduced (Figure 6H). These results suggest that the overexpression of *Zrsr1*, which reactivates minor intron splicing activity, prevents the progression of MASH.

Next, we aimed to investigate the therapeutic potential of targeting the IDH1-ammonia axis. Initially, we treated the mice with LOLA to suppress ammonia accumulation during MASH diet feeding (Figure 6I). Upon being harvest, the body weights of the LOLA-treated mice significantly decreased, whereas the liver weights had no difference (Figure S8H). The hepatic ammonia content was largely reduced in the mice after LOLA treatment, along with extensively decreased liver triglyceride and cholesterol contents, while the plasma triglyceride level was also suppressed. The plasma cholesterol level was unchanged (Figure 6J-K and Figure S8I). Liver histology presented improved hepatic steatosis, collagen deposition and ammonia accumulation (Figure 6L) in the mice treated with LOLA, while liver injury, as indicated by the ALT and AST levels, was reduced (Figure 6M). Additionally, hepatic fibrosis-, lipogenesis- and inflammation-related gene expression was suppressed (Figure 6N). These results indicated that reducing hepatic ammonia levels effectively ameliorates MASH progression. Then, we further investigated the potential therapeutic effect

of targeting IDH1. We treated the IDH1 inhibitor GSK864 in a MASH mouse model (Figure 6O). In mice fed with MASH diet, GSK864 treatment significantly decreased body weights, suppressed triglyceride levels in both the liver and plasma and ammonia content in the liver but did not affect liver weights or change plasma and hepatic cholesterol levels (Figure 6P-Q and Figure S8J-K). Notably, the MASH phenotypes, including lipid and ammonia accumulation, collagen deposition in the liver and liver injury, were substantially relieved upon GSK864 treatment (Figure 6R-S). Moreover, hepatic inflammation and fibrosis-related gene expression was extensively reduced. Consistent with previous results, GSK864 treatment significantly decreased the expression of the lipid marker *Fsp27* but did not alter lipogenic gene expression (Figure 6T). Taken together, these results strongly support that targeting the IDH1-ammonia axis is a promising therapeutic strategy for MASH therapy.

Discussion

Hepatic *de novo* lipogenesis is a fundamental metabolic process that is greatly elevated during MASLD progression. However, little is known regarding the preference for carbon sources in the liver during the activation of *de novo* lipogenesis in the MASH stage and its role in facilitating MASH progression. In this study, we revealed that hepatic minor intron splicing activity is obviously attenuated during MASH development and triggers SREBP1c-mediated *de novo* lipogenesis. Interestingly, in hepatic minor intron splicing-inactivated mice, amino acids, especially glutamine, are used as lipogenic carbons. Intriguingly,

glutamine is reductively carboxylated into citrate to support *de novo* lipogenesis. This metabolic rewiring may be a critical checkpoint for the MASH transition (Figure 6U). Several lines of evidence support this notion. First, the expression of the minor intron splicing factors *Zrsr1* and *Zrsr2* in the liver is drastically attenuated in mice with MASH and human MASH patients. In addition, it is synergistically downregulated by fatty acids and inflammatory cytokines, which are important pathogenic factors of MASH. A decrease in *Zrsr1* and *Zrsr2* results in compromised minor intron splicing activity. Second, mice with hepatic *Zrsr1* and *Zrsr2* depletion exhibited spontaneous hepatic steatosis and fibrosis phenotypes that were independent of dietary conditions. These two MASH signatures were further exacerbated upon HFD-induced insulin resistance and LXR activation. Notably, the minor introns of *Insig1* and *Insig2* are both retained, which results in the formation of prematurely terminated INSIG1 and INSIG2, thereby decreasing the anchoring of SREBP1c to the ER and inducing more extensive SREBP1c proteolytic activation. Interestingly, the decrease in the wild type *Insig1* transcript due to minor intron retention is more profound than that of *Insig2*, indicating that the dysfunction of Insig1 may be more important for proteolytic activation of SREBP1c than Insig2 under MASH condition. Importantly, we demonstrated that elevated SREBP1c activity is sufficient to drive the MASH phenotype under LXR activation, although SREBP2-mediated cholesterol metabolism is not obviously affected. Third, inactive minor intron splicing upon LXR activation leads to an increase in amino acid degradation instead of glycolysis. Additionally, metabolic flux analyses revealed an increase

in glutamine usage for lipid synthesis, suggesting that glutamine substantially replaces glucose as a dominant carbon source at the MASH stage. A recent study demonstrated that amino acids from dietary protein are a major carbon supplier for hepatic *de novo* lipogenesis, especially during MASLD progression (44). This discovery supports our findings, and we further revealed that minor intron retention is the key driver that leads to a significant shift in the carbon source utilization, from glucose to glutamine, under MASH condition. This point was further supported by the increase in glutaminolysis in MASH patients reported previously (45). Interestingly, we revealed that glutamine-derived lipogenic carbon is largely incorporated into monounsaturated fatty acids, suggesting that glutaminolysis at the MASH stage is specific for monounsaturated fatty acid synthesis. The unsaturation of fatty acids is enhanced in MASH, as previously reported (46). An increase in the amount of monounsaturated fatty acids may promote MASH/HCC progression by inhibiting ferroptosis (47). A previous report showed that ammonia accumulation induces *de novo* lipogenesis by activating SREBP1c in the liver (48). Here, we demonstrated that highly activated *de novo* lipogenesis caused by disrupted minor intron splicing generates ammonia accompanied by glutamine reductive carboxylation flux to facilitate stellate cell activation and exacerbate the fibrosis phenotype, which may form a positive feedback loop for MASH progression. However, the detailed mechanisms underlying the changes caused by minor intron retention in the preference for glutamine as a major carbon source and the exclusive generation of monounsaturated fatty acids in livers deficient in minor

intron splicing need further investigation. Interestingly, increased SREBP1c activity in minor intron splicing-deficient hepatocytes induces *Idh1* expression, which catalyzes the reductive carboxylation flux of cytosolic glutamine under certain conditions, such as hypoxia (25). This unique metabolic pathway is also frequently observed in cancer cells. In this study, we revealed that this reductive carboxylation route is activated by disrupted minor intron splicing during MASH progression. Enhanced *Idh1* levels were observed in the livers of ZLKO mice, and these changes were reversed by *Zrsr1* overexpression. Inhibition of IDH1 activity substantially blocked the induction of *de novo* lipogenesis in hepatocytes and hepatic steatosis, inflammation and especially fibrosis in mice with defective minor intron splicing. Finally, the overexpression of *Zrsr1* restored minor intron splicing activity and reversed aberrant *de novo* lipogenesis in MASH, thereby blocking MASH progression. More importantly, targeting the IDH1-ammonia axis via the clearance of ammonia accumulated in the liver and the inhibition of IDH1 activity profoundly suppressed MASH progression, thus providing convincing evidence that IDH1 activation-induced metabolic reprogramming could be a promising target for MASH therapy.

Taken together, our results suggest that disruption of minor intron splicing is a highly pivotal pathogenic factor for MASH progression. The effect of minor intron splicing inactivation may synergize with obesity-induced insulin resistance and LXR activation to trigger MASH pathogenesis. Notably, we revealed that minor intron splicing defects are induced by MASH pathogenic factors, which indicates

that inactivated minor intron splicing may be a critical checkpoint for irreversible liver damage in the MASH stage. Prevention of minor intron splicing inactivation and blockade of IDH1-ammonia-driven metabolic reprogramming during MASH progression may serve as a promising strategy for MASH therapy.

Materials and Methods

Sex as a biological variable

Our study examined male mice because male animals exhibited less variability in phenotype. However, the findings are expected to be relevant for both male and female animals.

Animal studies

All animal studies were performed according to procedures approved by the University Committee on the Use and Care of Animals at Shanghai Jiao Tong University. The animals' care was in accordance with institutional guidelines. C57BL/6J mice were maintained under 12/12 h light/dark cycles and fed regular rodent chow, high-fat diet (HFD) (D12492, Research Diets), low-fat diet (LFD) (D12450J, Research Diets) or choline-deficient L-amino-defined (CDA)-HFD (MASH diet) (A06071309, Research Diets). Wild-type (WT) C57BL/6J mice were purchased from Shanghai Lingchang Biotechnology, and *Cas9* knock-in mice were purchased from the JAX Laboratory (JAX stock 024858). For the generation of hepatic *Zrsr1* and *Zrsr2* double-deficient mice, we designed two small guide RNAs (sgRNAs) flanking the *Zrsr1* gene, which contains a single exon, and the

Zrsr2 gene within exon 1 and exon 2 via a CRISPR design web tool (http://crispr.mit.edu/) (49). Each sgRNA targeting *Zrsr1* and *Zrsr2* was cloned downstream of the U6 promoter, and two tandem U6-sgRNA cassettes were constructed into the adeno-associated virus (AAV) vector. *Zrsr1* and *Zrsr2* double-deficient mice were generated by transducing *Cas9* transgenic mice with a recombinant AAV vector expressing two sgRNAs targeting *Zrsr1* and *Zrsr2*. For AAV transduction, we injected approximately 1×10^{11} genome copies of AAV vectors per mouse via the tail vein. The AAV8 serotype was used for relative liver enrichment (50). For the oral gavage experiment, the two months old mice were orally administered a dose of 25 mg/kg T0901317 (Selleck, S7076) or 20 mg/kg SR9238 (MCE, HY-101442) dissolved in sunflower oil or sunflower oil alone for 4 days. For the ammonia clearance experiment, the mice were intraperitoneally injected with 2 g/kg L-ornithine-L-aspartate (LOLA) (Sigma, O7125) or saline every day for 17 days and then orally administered 25 mg/kg/day T0901317 for 4 days. For the GSK864 treatment, 75 mg/kg GSK864 (Selleck, S7994) was intraperitoneally injected into the mice before the oral administration of 25 mg/kg T0901317 (Selleck, S7076). For the LOLA and GSK864 treatment in a MASH model, 2 g/kg LOLA was administered through oral gavage and 75 mg/kg GSK864 was injected intraperitoneally on a daily basis during MASH diet feeding. More detailed information can be found in Supplemental Methods.

Statistical analysis

All the statistical analyses were performed via GraphPad Prism 9. Statistical differences were evaluated via two-tailed unpaired Student's t tests for comparisons between two groups or analysis of variance (ANOVA) and appropriate post hoc analyses for comparisons of more than two groups. A p value of less than 0.05 (*$p < 0.05$, **$p < 0.01$, and ***$p < 0.001$) was considered to indicate statistical significance. The statistical methods and corresponding p values for the data shown in each panel are included in the figure legends.

Study approval

Human liver biopsies from MASH patients and healthy liver transplant donors were obtained from Shanghai Renji Hospital. All the research was conducted in accordance with both the Declarations of Helsinki and Istanbul. All the research was approved by the Institutional Review Board of Renji Hospital affiliated to Shanghai Jiao Tong University School of Medicine (IRB Reference Number: KY2020-190), and written consent was given in writing by all the subjects after the nature and possible consequences of the studies were explained.

Data availability

The RNA-seq data files have been deposited in the Gene Expression Omnibus (www.ncbi.nlm.nih.gov/geo/) under accession numbers GSE252030 and GSE272322. Values for all data points in graphs are reported in the Supporting Data Values file. The data generated in this study are available upon request from the corresponding author.

Author contributions

Y.F., X.P., H.S., X.L., Y.Z., J.T., Y.L., D.C., W.L., J.Z. and X.Y.Z. conceived the project and designed the research. Y.F. performed the majority of the studies. X.P., H.S., Y.L., D.C., and W.L. performed some animal and cell experiments. Y.F., J.M., M.H., Y.M. and X.Y.Z. analyzed the data and wrote the manuscript.

Acknowledgments

We appreciate Dr. Xuelian Xiong from Zhongshan Hospital, Fudan University in Shanghai, for providing the HSC cell line and Dr. Yu Li from the Shanghai Institute of Nutrition and Health of the Chinese Academy of Sciences for providing the Insig1 adenovirus. We are grateful to Mr. Huahua Song from the Core Facility of Basic Medical Sciences, Shanghai Jiao Tong University School of Medicine, for assisting with the radioactive isotope experiments and Ms. Junyao Wang from the Institutional Center for Shared Technologies and Facilities of SINH, CAS for technical assistance with the metabolic flux analyses. We thank the Zhao laboratory members for their detailed guidance and advice on this study.

Funding: This work was supported by the National Key R&D Program of China (2023YFA1800802, 2020YFA0803603 to X.Y.Z. and 2022YFC3502101, 2022YFC3502100 to Y.M.), the National Natural Science Foundation of China (82070894 to X.Y.Z. and 82270619, 81970513 to Y.M.), and the Science and Technology Commission of Shanghai Municipality (21ZR1436500, 22ZR1479800

to X.Y.Z.). Shanghai Frontiers Science Center of Cellular Homeostasis and Human Diseases. Innovative research team of high-level local universities in Shanghai (SHSMU-ZDCX20212501 to X.Y.Z.), Clinical Research Innovation and Development Fund of Renji Hospital, School of Medicine, Shanghai Jiao Tong University (PY120-05 to Y.M.), and the Major Project of National Thirteenth Five Plan (2017ZX09304016 to Y.M.).

References

1. Cohen JC, Horton JD, and Hobbs HH. Human fatty liver disease: old questions and new insights. *Science.* 2011;332(6037):1519-23.
2. Machado MV, and Diehl AM. Pathogenesis of Nonalcoholic Steatohepatitis. *Gastroenterology.* 2016;150(8):1769-77.
3. Rinella ME. Nonalcoholic fatty liver disease: a systematic review. *JAMA.* 2015;313(22):2263-73.
4. Riazi K, Azhari H, Charette JH, Underwood FE, King JA, Afshar EE, et al. The prevalence and incidence of NAFLD worldwide: a systematic review and meta-analysis. *Lancet Gastroenterol Hepatol.* 2022;7(9):851-61.
5. Friedman SL, Neuschwander-Tetri BA, Rinella M, and Sanyal AJ. Mechanisms of NAFLD development and therapeutic strategies. *Nat Med.* 2018;24(7):908-22.
6. Neuschwander-Tetri BA. Hepatic lipotoxicity and the pathogenesis of nonalcoholic steatohepatitis: the central role of nontriglyceride fatty acid metabolites. *Hepatology.* 2010;52(2):774-88.

7. Samuel VT, and Shulman GI. Nonalcoholic Fatty Liver Disease as a Nexus of Metabolic and Hepatic Diseases. *Cell Metab.* 2017.
8. Sunny NE, Bril F, and Cusi K. Mitochondrial Adaptation in Nonalcoholic Fatty Liver Disease: Novel Mechanisms and Treatment Strategies. *Trends Endocrinol Metab.* 2017;28(4):250-60.
9. Tilg H, and Moschen AR. Evolution of inflammation in nonalcoholic fatty liver disease: the multiple parallel hits hypothesis. *Hepatology.* 2010;52(5):1836-46.
10. Shenasa H, and Bentley DL. Pre-mRNA splicing and its cotranscriptional connections. *Trends Genet.* 2023;39(9):672-85.
11. Nilsen TW, and Graveley BR. Expansion of the eukaryotic proteome by alternative splicing. *Nature.* 2010;463(7280):457-63.
12. Bradley RK, and Anczuków O. RNA splicing dysregulation and the hallmarks of cancer. *Nat Rev Cancer.* 2023;23(3):135-55.
13. Montes M, Sanford BL, Comiskey DF, and Chandler DS. RNA Splicing and Disease: Animal Models to Therapies. *Trends Genet.* 2019;35(1):68-87.
14. El Marabti E, Malek J, and Younis I. Minor Intron Splicing from Basic Science to Disease. *Int J Mol Sci.* 2021;22(11).
15. Xu K, Wu T, Xia P, Chen X, and Yuan Y. Alternative splicing: a bridge connecting NAFLD and HCC. *Trends Mol Med.* 2023;29(10):859-72.
16. Wu P, Zhang M, and Webster NJG. Alternative RNA Splicing in Fatty Liver Disease. *Front Endocrinol (Lausanne).* 2021;12:613213.

17. Li Y, Xu J, Lu Y, Bian H, Yang L, Wu H, et al. DRAK2 aggravates nonalcoholic fatty liver disease progression through SRSF6-associated RNA alternative splicing. *Cell Metab.* 2021;33(10):2004-20 e9.

18. Madan V, Kanojia D, Li J, Okamoto R, Sato-Otsubo A, Kohlmann A, et al. Aberrant splicing of U12-type introns is the hallmark of ZRSR2 mutant myelodysplastic syndrome. *Nat Commun.* 2015;6:6042.

19. Weinstein R, Bishop K, Broadbridge E, Yu K, Carrington B, Elkahloun A, et al. Zrsr2 Is Essential for the Embryonic Development and Splicing of Minor Introns in RNA and Protein Processing Genes in Zebrafish. *Int J Mol Sci.* 2022;23(18).

20. Gómez-Redondo I, Ramos-Ibeas P, Pericuesta E, Fernández-González R, Laguna-Barraza R, and Gutiérrez-Adán A. Minor Splicing Factors Zrsr1 and Zrsr2 Are Essential for Early Embryo Development and 2-Cell-Like Conversion. *Int J Mol Sci.* 2020;21(11).

21. Joh K, Matsuhisa F, Kitajima S, Nishioka K, Higashimoto K, Yatsuki H, et al. Growing oocyte-specific transcription-dependent de novo DNA methylation at the imprinted Zrsr1-DMR. *Epigenetics Chromatin.* 2018;11(1):28.

22. Horiuchi K, Perez-Cerezales S, Papasaikas P, Ramos-Ibeas P, Lopez-Cardona AP, Laguna-Barraza R, et al. Impaired Spermatogenesis, Muscle, and Erythrocyte Function in U12 Intron Splicing-Defective Zrsr1 Mutant Mice. *Cell Rep.* 2018;23(1):143-55.

23. Alén F, Gómez-Redondo I, Rivera P, Suárez J, Ramos-Ibeas P, Pericuesta E, et al. Sex-Dimorphic Behavioral Alterations and Altered Neurogenesis in U12 Intron Splicing-Defective Zrsr1 Mutant Mice. *Int J Mol Sci.* 2019;20(14).
24. Nishimura K, Yamazaki H, Zang W, and Inoue D. Dysregulated minor intron splicing in cancer. *Cancer Sci.* 2022;113(9):2934-42.
25. Metallo CM, Gameiro PA, Bell EL, Mattaini KR, Yang J, Hiller K, et al. Reductive glutamine metabolism by IDH1 mediates lipogenesis under hypoxia. *Nature.* 2011;481(7381):380-4.
26. Li T, and Le A. Glutamine Metabolism in Cancer. *Adv Exp Med Biol.* 2018;1063:13-32.
27. Yang L, Venneti S, and Nagrath D. Glutaminolysis: A Hallmark of Cancer Metabolism. *Annu Rev Biomed Eng.* 2017;19:163-94.
28. Kohjima M, Higuchi N, Kato M, Kotoh K, Yoshimoto T, Fujino T, et al. SREBP-1c, regulated by the insulin and AMPK signaling pathways, plays a role in nonalcoholic fatty liver disease. *Int J Mol Med.* 2008;21(4):507-11.
29. Shimomura I, Bashmakov Y, and Horton JD. Increased levels of nuclear SREBP-1c associated with fatty livers in two mouse models of diabetes mellitus. *J Biol Chem.* 1999;274(42):30028-32.
30. Brown MS, Radhakrishnan A, and Goldstein JL. Retrospective on Cholesterol Homeostasis: The Central Role of Scap. *Annu Rev Biochem.* 2017.

31. Calkin AC, and Tontonoz P. Transcriptional integration of metabolism by the nuclear sterol-activated receptors LXR and FXR. *Nat Rev Mol Cell Biol.* 2012;13(4):213-24.

32. Zhao XY, Xiong X, Liu T, Mi L, Peng X, Rui C, et al. Long noncoding RNA licensing of obesity-linked hepatic lipogenesis and NAFLD pathogenesis. *Nat Commun.* 2018;9(1):2986.

33. Griffett K, and Burris TP. Development of LXR inverse agonists to treat MAFLD, NASH, and other metabolic diseases. *Front Med (Lausanne).* 2023;10:1102469.

34. Sun LP, Li L, Goldstein JL, and Brown MS. Insig required for sterol-mediated inhibition of Scap/SREBP binding to COPII proteins in vitro. *J Biol Chem.* 2005;280(28):26483-90.

35. Radhakrishnan A, Ikeda Y, Kwon HJ, Brown MS, and Goldstein JL. Sterol-regulated transport of SREBPs from endoplasmic reticulum to Golgi: oxysterols block transport by binding to Insig. *Proc Natl Acad Sci U S A.* 2007;104(16):6511-8.

36. Feramisco JD, Goldstein JL, and Brown MS. Membrane topology of human insig-1, a protein regulator of lipid synthesis. *J Biol Chem.* 2004;279(9):8487-96.

37. Yabe D, Brown MS, and Goldstein JL. Insig-2, a second endoplasmic reticulum protein that binds SCAP and blocks export of sterol regulatory element-binding proteins. *Proc Natl Acad Sci U S A.* 2002;99(20):12753-8.

38. Azzu V, Vacca M, Kamzolas I, Hall Z, Leslie J, Carobbio S, et al. Suppression of insulin-induced gene 1 (INSIG1) function promotes hepatic lipid remodelling and restrains NASH progression. *Mol Metab.* 2021;48:101210.

39. Xu D, Wang Z, Xia Y, Shao F, Xia W, Wei Y, et al. The gluconeogenic enzyme PCK1 phosphorylates INSIG1/2 for lipogenesis. *Nature.* 2020;580(7804):530-5.

40. Moyer DC, Larue GE, Hershberger CE, Roy SW, and Padgett RA. Comprehensive database and evolutionary dynamics of U12-type introns. *Nucleic Acids Res.* 2020;48(13):7066-78.

41. Madan V, Cao Z, Teoh WW, Dakle P, Han L, Shyamsunder P, et al. ZRSR1 co-operates with ZRSR2 in regulating splicing of U12-type introns in murine hematopoietic cells. *Haematologica.* 2022;107(3):680-9.

42. Ricoult SJ, Dibble CC, Asara JM, and Manning BD. Sterol Regulatory Element Binding Protein Regulates the Expression and Metabolic Functions of Wild-Type and Oncogenic IDH1. *Mol Cell Biol.* 2016;36(18):2384-95.

43. Wang ZX, Wang MY, Yang RX, Zhao ZH, Xin FZ, Li Y, et al. Ammonia Scavenger Restores Liver and Muscle Injury in a Mouse Model of Non-alcoholic Steatohepatitis With Sarcopenic Obesity. *Front Nutr.* 2022;9:808497.

44. Liao Y, Chen Q, Liu L, Huang H, Sun J, Bai X, et al. Amino acid is a major carbon source for hepatic lipogenesis. *Cell Metab.* 2024;36(11):2437-48 e8.

45. Du K, Chitneni SK, Suzuki A, Wang Y, Henao R, Hyun J, et al. Increased Glutaminolysis Marks Active Scarring in Nonalcoholic Steatohepatitis Progression. *Cell Mol Gastroenterol Hepatol.* 2020;10(1):1-21.

46. Juárez-Hernández E, Chávez-Tapia NC, Uribe M, and Barbero-Becerra VJ. Role of bioactive fatty acids in nonalcoholic fatty liver disease. *Nutr J.* 2016;15(1):72.

47. Li Z, Liao X, Hu Y, Li M, Tang M, Zhang S, et al. SLC27A4-mediated selective uptake of mono-unsaturated fatty acids promotes ferroptosis defense in hepatocellular carcinoma. *Free Radic Biol Med.* 2023;201:41-54.

48. Cheng C, Geng F, Li Z, Zhong Y, Wang H, Cheng X, et al. Ammonia stimulates SCAP/Insig dissociation and SREBP-1 activation to promote lipogenesis and tumour growth. *Nat Metab.* 2022;4(5):575-88.

49. Ran FA, Hsu PD, Wright J, Agarwala V, Scott DA, and Zhang F. Genome engineering using the CRISPR-Cas9 system. *Nature protocols.* 2013;8(11):2281-308.

50. Issa SS, Shaimardanova AA, Solovyeva VV, and Rizvanov AA. Various AAV Serotypes and Their Applications in Gene Therapy: An Overview. *Cells.* 2023;12(5).

FIGURES

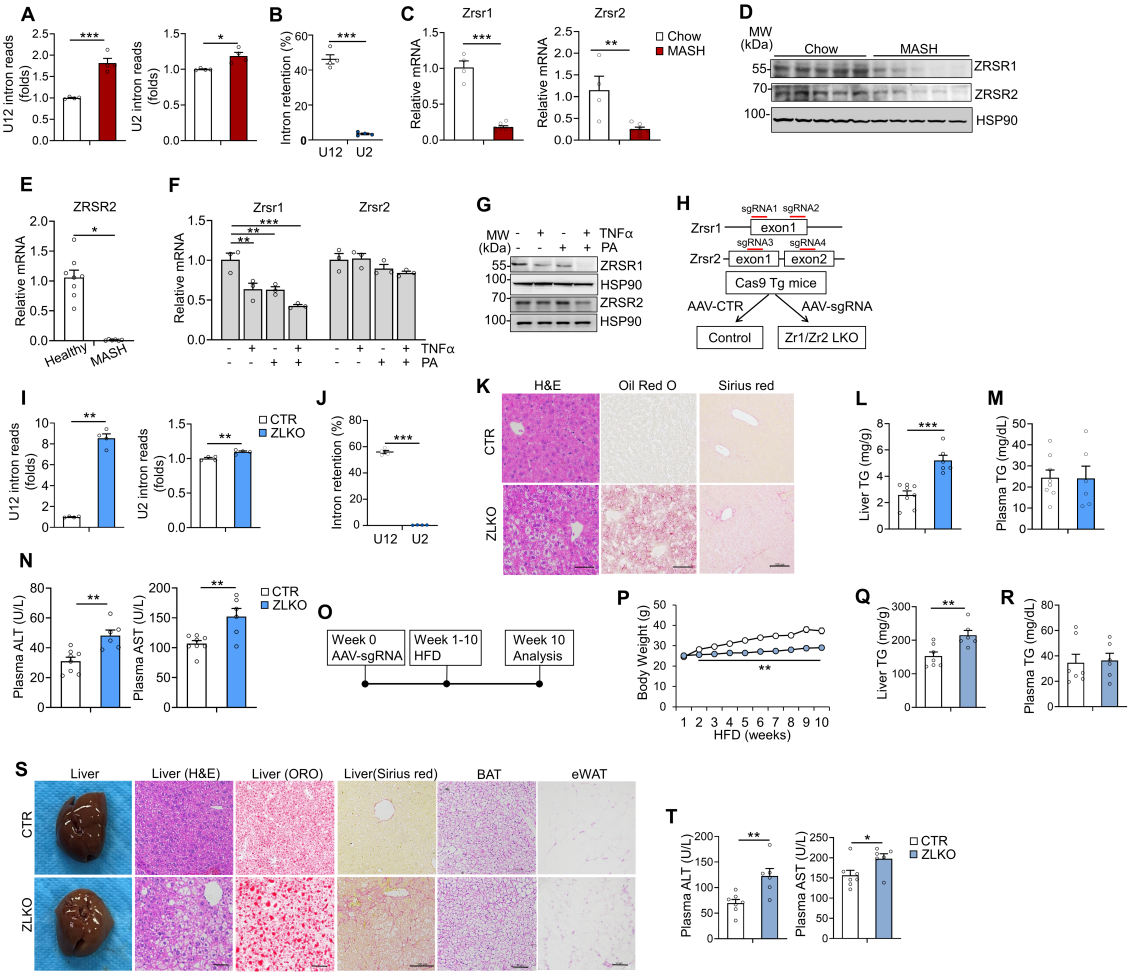

Figure 1. Inactivation of minor intron splicing caused by decrease in Zrsr1 and Zrsr2 expression in the liver induces MASH phenotype

(**A**) Fold change of minor (U12) and major (U2) intron reads of the livers of mice after chow (*n*=4) and CDA-HFD (MASH diet, *n*=4) feeding for 6 months. (**B**) Percentages of U12 and U2 retained introns. (**C-D**) QPCR (**C**) and immunoblotting (**D**) analyses of Zrsr1 and Zrsr2 expression in the livers of mice fed chow diet (*n*=4) or MASH diet (*n*=7). (**E**) QPCR analysis of ZRSR2 expression in liver samples from healthy controls (*n*=8) and MASH patients (*n*=6). (**F-G**) QPCR (**F**) and immunoblotting (**G**) analysis of Zrsr1 and Zrsr2 expression in primary hepatocytes (*n*=3) treated with vehicle, 50 μM TNFα or 0.1 mM palmitic acid (PA) alone or in combination for 24 h. (**H**) Schematic diagram of

the strategy used to generate Zrsr1 and Zrsr2 double-deficient mice via CRISPR/CAS9. (**I**) Fold change of U12 and U2 intron reads of the livers of AAV-control- (CTR, *n*=4) and Zrsr1- and Zrsr2-sgRNA-injected Cas9-Tg mice (ZLKO, *n*=4) on chow-diet feeding. (**J**) Percentages of U12 and U2 retained introns. (**K**) H&E staining, Oil Red O staining and Sirius red staining (scale bar=100 μm). (**L-M**) Liver (**L**) and plasma (**M**) triglyceride (TG) contents in CTR (*n*=8) and ZLKO mice (*n*=6). (**N**) Plasma ALT and AST levels. (**O**) Diagram of the study design. (**P**) Body weight curves of CTR (*n*=7) and ZLKO (*n*=6) mice fed high-fat diet (HFD) for 10 weeks. (**Q**-**R**) Liver (**Q**) and plasma (**R**) TG contents. (**S**) General morphology, H&E staining, Oil Red O staining and Sirius red staining of liver tissue and H&E staining of fat tissue (scale bar=100μm). (**T**) Plasma ALT and AST levels. The data are presented as the mean ± SEM. *p < 0.05, **p < 0.01, ***p < 0.001 by two-tailed unpaired Student's t-test (A-C, E, I-J, L-N, Q-R and T), by two-way ANOVA with multiple comparisons (P), by one-way ANOVA with Dunnett's test (F).

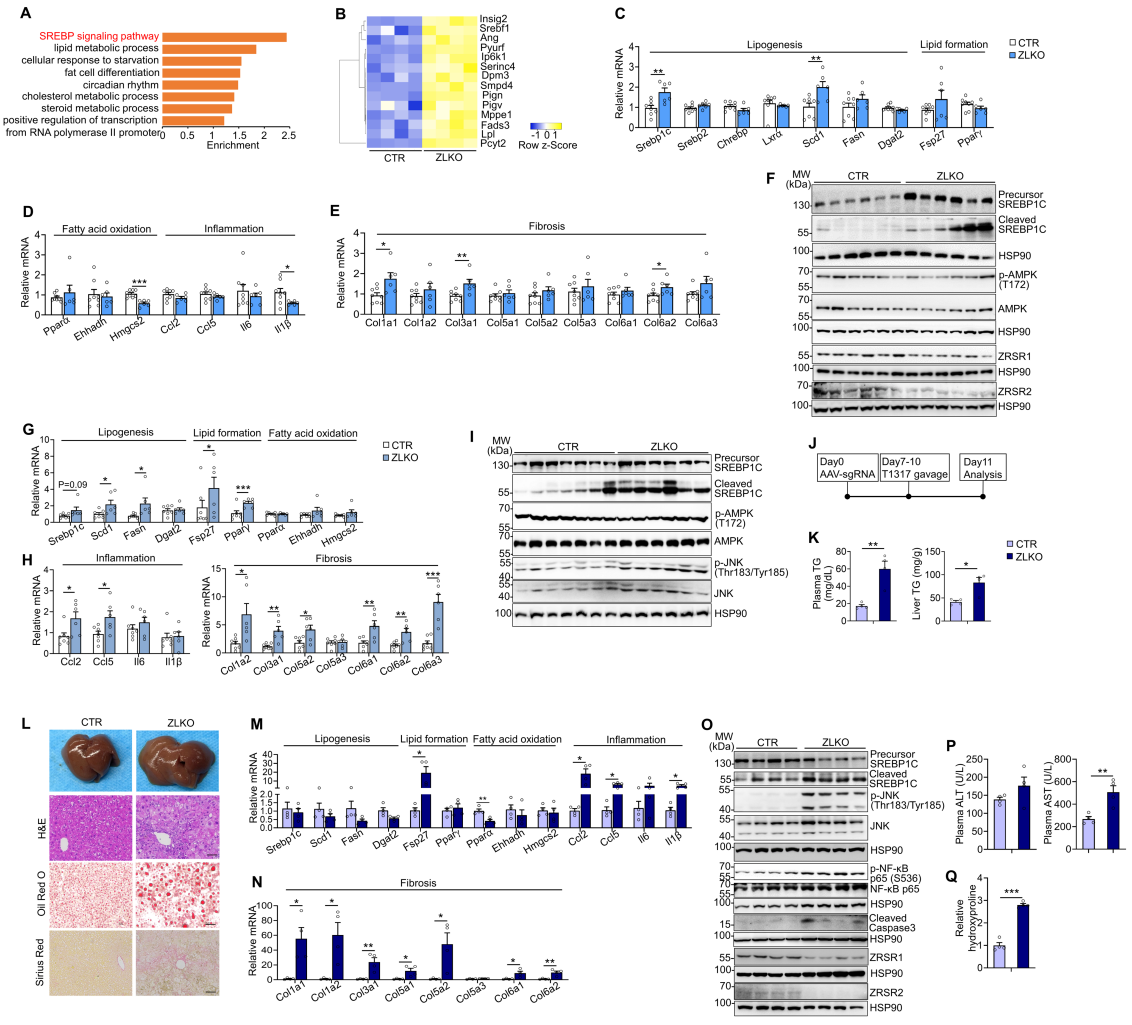

Figure 2. Minor intron splicing deficiency activates SREBP1c-mediated *de novo* lipogenesis, which facilitates the MASH progression under LXR activation.

(**A**) Gene Ontology analysis showing enriched pathways associated with genes upregulated in the livers of ZLKO mice (*n*=4) compared to those in CTR mice (*n*=4) on chow-diet feeding. (**B**) Heatmap showing a set of lipogenic genes whose expression is upregulated in the livers of ZLKO mice on chow-diet feeding. (**C-E**) QPCR analysis of hepatic genes involved in lipogenesis, lipid formation (**C**), fatty acid oxidation, and inflammation (**D**) and fibrosis (**E**) in CTR (*n*=8) and ZLKO (*n*=6) mice. (**F**) Immunoblotting of liver lysates from CTR and ZLKO mice. (**G-H**) QPCR analysis of hepatic genes involved in lipid metabolism (**G**), inflammation and fibrosis (**H**) in CTR (*n*=7) and ZLKO (*n*=6) mice after high-

fat diet (HFD) feeding. (**I**) Immunoblotting of liver lysates from CTR and ZLKO mice after HFD feeding. (**J**) Diagram of the study design. (**K**) Plasma (left) and liver (right) triglyceride (TG) contents of CTR (*n*=4) and ZLKO (*n*=4) mice receiving oral gavage of 25 mg/kg/day T0901317 (T1317) for 4 days. (**L**) General morphology, H&E staining, Oil Red O staining, and Sirius red staining (scale bar=100 μm). (**M**-**N**) QPCR analysis of hepatic genes involved in lipid metabolism, inflammation (**M**) and fibrosis (**N**). (**O**) Immunoblotting of liver lysates from CTR and ZLKO mice. (**P**-**Q**) Plasma ALT and AST levels (**P**) and liver hydroxyproline content (**Q**). The data are presented as the mean ± SEM. *p < 0.05, **p < 0.01, ***p < 0.001 by two-tailed unpaired Student's t-test (C-E, G-H, K, M-N, P-Q).

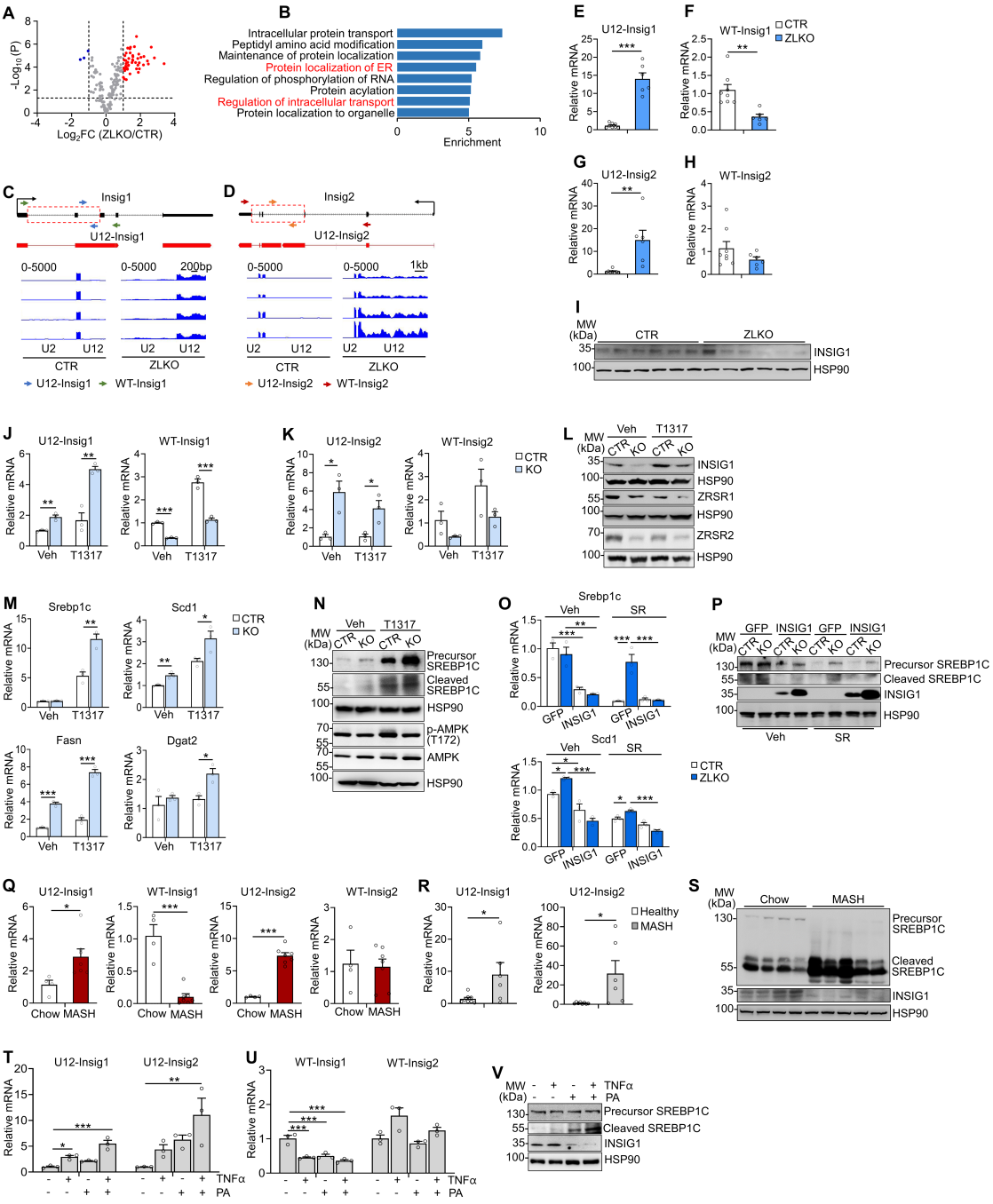

Figure 3. Disruption of minor intron splicing leads to minor intron retention of *Insig1* and *Insig2*, which mediates proteolytic activation of SREBP1c. (**A**) Volcano plot showing the upregulated (red) and downregulated (blue) minor intron retention genes in the livers of ZLKO mice (*n*=4) compared with those of CTR mice (*n*=4) on chow-diet feeding. (**B**) Gene Ontology analysis showing pathways enriched in minor intron retention genes. (**C-D**) Genome browser

showing peaks corresponding to the U12 and U2 introns in Insig1 and Insig2 from the livers of CTR (*n*=4) and ZLKO (*n*=4) mice. (**E**-**H**) QPCR analysis of the U12 intron expression of Insig1 and Insig2 (**E**, **G**) and the mRNA levels of the wild type (WT) Insig1 and Insig2 (**F**, **H**) in the livers of CTR (*n*=8) and ZLKO (*n*=6) mice. The primers used are shown in **C**-**D**. (**I**) Immunoblotting of liver lysates from CTR and ZLKO mice. (**J**-**K**) QPCR analysis of the U12 intron and WT mRNA expression of Insig1 (**J**) and Insig2 (**K**) in the control (CTR, *n*=3) and Zrsr1 and Zrsr2 knockout AML12 cells via CRISPR/CAS9 (KO, *n*=3) treated with vehicle (Veh) or T0901317 (T1317, 5 μM) for 24 h. (**L**) Immunoblotting of lysates from CTR and KO AML12 cells. (**M**) QPCR analysis of lipogenic genes in CTR and KO AML12 cells. (**N**) Immunoblotting of lysates from cells in **M**. (**O**) Primary hepatocytes (*n*=3) were isolated from the livers of CTR and ZLKO mice and infected with GFP and Insig1 adenoviruses. The expression of lipogenic genes was measured by qPCR after vehicle (Veh) or SR9238 (10 μM, SR) treatment for 24 h. (**P**) Immunoblotting of lysates from cells in **O**. (**Q**) QPCR analysis of U12 introns and WT mRNA expression of Insig1 and Insig2 in the livers of mice fed chow diet (*n*=4) or MASH diet (*n*=7) for 6 months. (**R**) QPCR analysis of U12 introns in Insig1 and Insig2 in liver samples from healthy controls (*n*=8) and MASH patients (*n*=6). (**S**) Immunoblotting analysis of liver lysates from mice fed chow or MASH diet. (**T**-**U**) QPCR analysis of U12 intron (**T**) and the WT mRNA expression (**U**) of Insig1 and Insig2 in primary hepatocytes (*n*=3) treated with vehicle, 50 μM TNFα or 0.1 mM palmitic acid (PA) alone or in combination for 24 h. (**V**) Immunoblotting of cell lysates in **T**-**U**. The data are presented as the mean ± SEM. *p < 0.05, **p < 0.01, ***p < 0.001 by two-tailed unpaired Student's t test (E-H, J-K, M and Q-R), by two-way ANOVA with multiple comparisons (O), by one-way ANOVA with Dunnett's test (T-U).

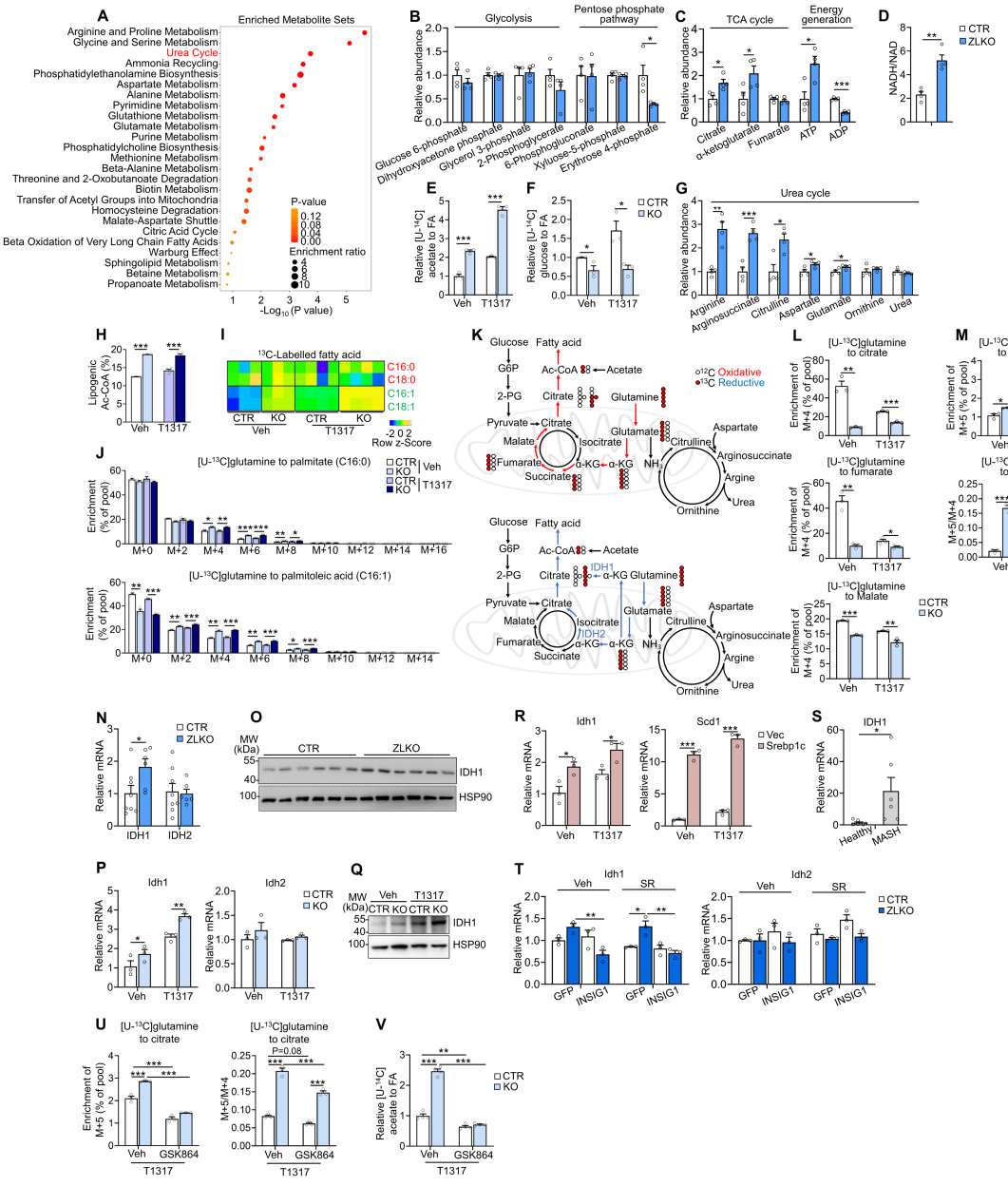

Figure 4. Dysfunction of minor intron splicing activates reductive glutamine metabolism for *de novo* lipogenesis by inducing Idh1 expression.

(**A**) Clustering analysis performed by MetaboAnalyst showing the enriched metabolic pathways associated with the upregulated metabolites in the livers of ZLKO mice (*n*=4) compared with those of CTR mice (*n*=4) after receiving oral gavage of T0901317 (T1317, 25 mg/kg/day) for 4 days. (**B**-**C**) The levels of metabolites involved in glycolysis, the pentose phosphate pathway (**B**), the TCA cycle, and energy generation (**C**) were measured via metabolomics. (**D**) NADH

and NAD levels were measured, and the NADH-to-NAD ratio was calculated. (**E-F**) The incorporation of [U-^{14}C]acetate acid (**E**) and [U-^{14}C]glucose (**F**) into lipids was measured in CTR and KO AML12 cells (*n*=3) after vehicle (Veh) or T1317 (5 μM) treatment for 24 h. (**G**) Metabolites involved in the urea cycle pathway were measured via metabolomics. (**H**) The enrichment of lipogenic acetyl-CoA was calculated via FAMetA in CTR and KO AML12 cells cultured with [U-^{13}C]glutamine for 24 h and then treated with Veh (*n*=3) or 5 μM T1317 (*n*=4) for 24 h. (**I**) Heatmap representing the enrichment of ^{13}C-labeled fatty acids in CTR and KO AML12 cells. (**J**) Mass isotopologue distribution analysis of palmitate and palmitoleic acid in CTR and KO AML12 cells (*n*=3). (**K**) Schematic diagram showing the oxidative (red) and reductive (blue) metabolic flux of [U-^{13}C]glutamine. (**L-M**) Mass isotopologue distribution analysis of citrate, fumarate, and malate (M+4) (**L**) and citrate (M+5) and the ratio of M+5 to M+4-labeled citrate (**M**) in CTR and KO AML12 cells (*n*=3). (**N**) QPCR analysis of Idh1 and Idh2 expression in the livers of CTR (*n*=8) and ZLKO (*n*=6) mice fed a normal chow diet. (**O**) Immunoblotting analysis of liver lysates from **N**. (**P**) QPCR analysis of Idh1 and Idh2 expression in CTR and KO AML12 cells (*n*=3) treated with Veh or T1317 (5 μM) for 24 h. (**Q**) Immunoblotting analysis of cell lysates from **P**. (**R**) QPCR analysis of Idh1 and Scd1 expression in AML12 cells stably overexpressing vector (Vec, *n*=3) or Srebp1c (*n*=3) after Veh and T1317 treatment. (**S**) QPCR analysis of Idh1 expression in liver samples from healthy controls (*n*=8) and MASH patients (*n*=6). (**T**) Primary hepatocytes (*n*=3) were isolated from CTR and ZLKO mouse livers and infected with GFP and Insig1 adenoviruses. The expression of Idh1 and Idh2 was measured by qPCR after Veh or SR9238 (10 μM, SR) treatment for 24 h. (**U**) Mass isotopologue distribution analysis of citrate (M+5) and the ratio of M+5 to M+4-labeled citrate in CTR and KO AML12 cells (*n*=3) cultured with [U-^{13}C]glutamine and treated with T1317 (5 μM) in combination with Veh and GSK864 (10 μM) for 24 h. (**V**) Incorporation of [U-^{14}C]acetate into lipids. The data are presented as the mean ± SEM. *p<0.05, **p < 0.01, ***p < 0.001 by two-tailed unpaired Student's t-test (B-H, J, L-N, P, and R-S), by two-way ANOVA with multiple comparisons (T-V).

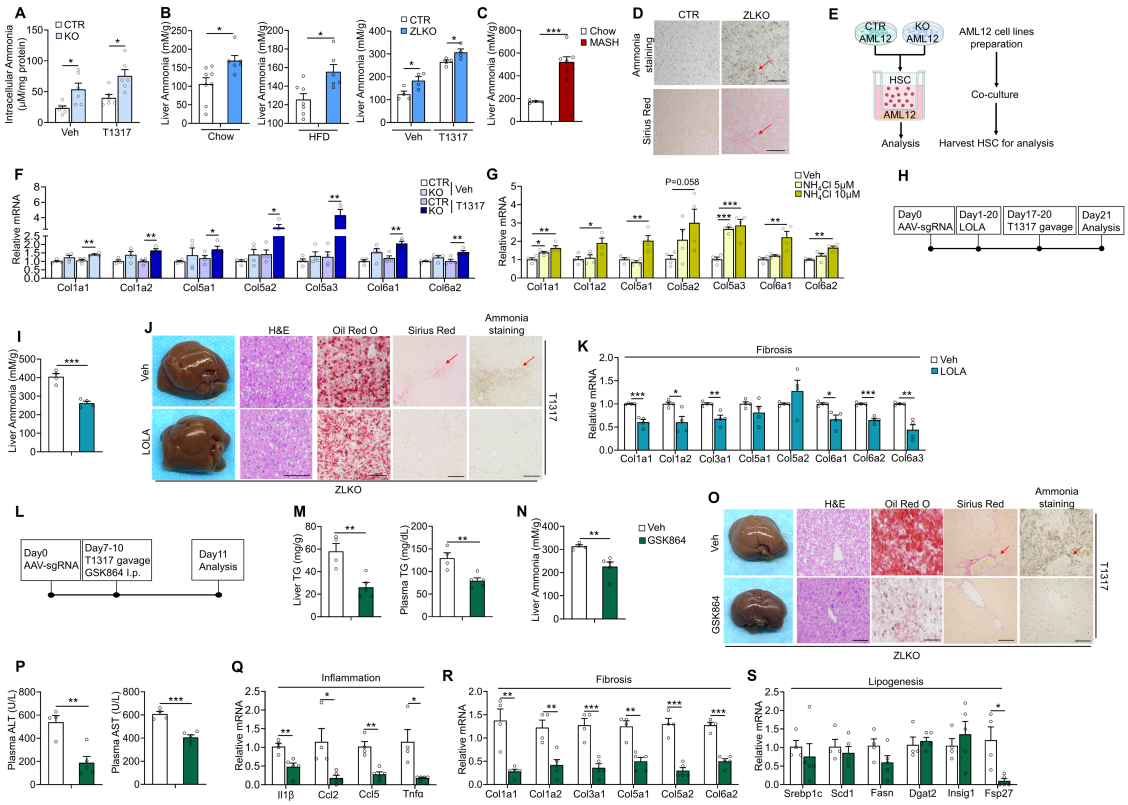

Figure 5. IDH1 induces ammonia accumulation in the liver, which triggers hepatic stellate cell activation to drive hepatic fibrogenesis.

(**A**) Ammonia levels were measured in CTR and KO AML12 cells (*n*=6) after vehicle (Veh) or T0901317 (T1317, 5 μM) treatment for 24 h. (**B**) Ammonia levels were measured in the livers of CTR and ZLKO mice after feeding chow diet (left, CTR, *n*=8, ZLKO, *n*=6), high-fat diet (middle, CTR, *n*=7, ZLKO, *n*=6) or oral gavage of vehicle or T1317 (25 mg/kg/day) for 4 days (right, CTR, *n*=4, ZLKO, *n*=4). (**C**) Ammonia levels were measured in the livers of mice fed chow diet (*n*=4) or CDA-HFD (MASH diet, *n*=7) for 6 months. (**D**) Ammonia staining and Sirius red staining of livers from CTR and ZLKO mice treated with T1317 (scale bar=100μm). (**E**) Schematic diagram showing the strategy of co-culture of CTR and KO AML12 cells with hepatic stellate cells (HSCs). (**F**) QPCR analysis of genes involved in fibrosis in co-cultured HSCs (*n*=4). (**G**) QPCR analysis of fibrotic genes in HSCs (*n*=4) treated with Veh or 5μM or 10μM NH_4Cl for 24 h. (**H**) Diagram of the study design. (**I**) Ammonia levels were measured in the livers

of ZLKO mice daily intraperitoneally injected with vehicle (Veh, *n*=4) or 2 g/kg/day L-ornithine-aspartate (LOLA, *n*=4) for 17 days and then combined with an oral administration of T1317 (25mg/kg/day) for 4 days. (**J**) General morphology, H&E staining, Oil Red O staining, Sirius red staining and ammonia staining (scale bar=100μm). (**K**) QPCR analysis of hepatic genes involved in fibrosis. (**L**) Diagram of the study design. (**M**-**N**) Liver and plasma triglyceride (TG) content (**M**) and hepatic ammonia contents (**N**) in ZLKO mice intraperitoneally injected with Veh (*n*=4) or GSK864 (75 mg/kg/day, *n*=5) combined with an oral administration of T1317 (25 mg/kg/day) for 4 days. (**O**) General morphology, H&E staining, Oil Red O staining, Sirius red staining and ammonia staining (scale bar=100μm). (**P**) Plasma ALT and AST levels. (**Q**-**S**) QPCR analysis of hepatic genes involved in inflammation (**Q**), fibrosis (**R**) and lipogenesis (**S**). The red arrow in **D**, **J** and **O** indicates the area where collagen and ammonia accumulated. The data are presented as the mean ± SEM. *p<0.05, **p < 0.01, ***p < 0.001 by two-tailed unpaired Student's t-test (A-C, F, I, K, M-N, P-S), by one-way ANOVA with Dunnett's test (G).

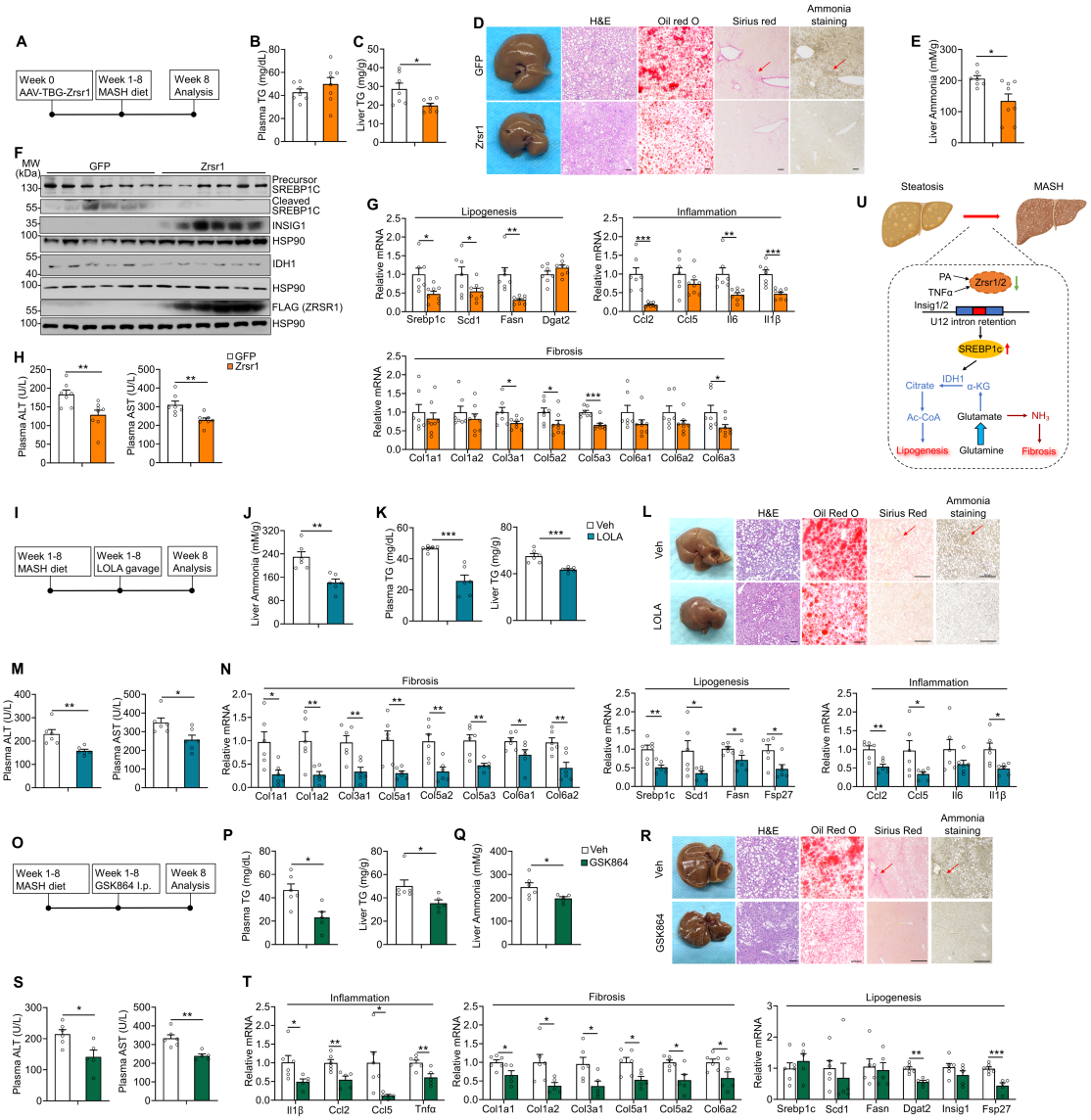

Figure 6. Reactivating minor intron splicing or blocking the IDH1-ammonia axis ameliorates MASH progression.

(**A**) Diagram of the study design. (**B-C**) Plasma (**B**) and liver (**C**) triglyceride (TG) contents of mice injected with AAV-TBG-GFP (GFP, *n*=7) or AAV-TBG-Zrsr1 (Zrsr1, *n*=8) after CDA-HFD (MASH diet) feeding for 8 weeks. (**D**) General morphology, hematoxylin and eosin (H&E) staining, Oil Red O staining, Sirius red staining and ammonia staining (scale bar=100μm). (**E-F**) Liver ammonia levels (**E**) and immunoblotting of liver lysates (**F**) was measured. (**G**) QPCR analysis of hepatic genes involved in lipogenesis, inflammation and fibrosis. (**H**) Plasma ALT

and AST levels. (**I**) Diagram of the study design. (**J**) Hepatic ammonia levels in wild type mice administrated with saline (*n*=6) or 2 g/kg/day L-ornithine-aspartate (LOLA, *n*=6) daily through oral gavage, and both groups were fed on MASH diet for 8 weeks. (**K**) Plasma (left) and liver (right) triglyceride (TG) contents. (**L**) General morphology, H&E staining, Oil Red O staining, Sirius red staining and ammonia staining (scale bar=100μm). (**M**) Plasma ALT and AST levels. (**N**) QPCR analysis of hepatic genes involved in fibrosis (left), lipogenesis (middle) and inflammation (right). (**O**) Diagram of the study design. (**P**) Plasma (left) and liver (right) TG contents in wild type mice intraperitoneally injected daily with vehicle (Veh, *n*=6) or 75 mg/kg/day GSK864 (*n*=5), and both groups were fed on MASH diet for 8 weeks. (**Q**) Hepatic ammonia content. (**R**) General morphology, H&E staining, Oil Red O staining, Sirius red staining and ammonia staining (scale bar=100μm). (**S**) Plasma ALT and AST levels. (**T**) QPCR analysis of hepatic genes involved in inflammation (left), fibrosis (middle) and lipogenesis (right). (**U**) Schematic illustration of the mechanism of the MASH progression by which disruption of minor intron splicing caused by the reduction of Zrsr1 and Zrsr2 triggers SREBP1c-dependent IDH1-mediated glutamine reductive carboxylation flux for *de novo* lipogenesis, thus activating hepatic stellate cells via excessive ammonia production. The red arrow in **D**, **L** and **R** indicates the area where collagen and ammonia accumulated. The data are presented as the mean ± SEM. *p<0.05, **p < 0.01, ***p < 0.001 by two-tailed unpaired Student's t-test (B-C, E, G-H, J-K, M-N, P-Q and S-T).